



Link auxiliary field method in the extended Hubbard model

Sergey Mostovoy * and Oleg Pavlovsky †

Faculty of Physics, Moscow State University, Moscow, 119991, Russia
and National Research Center “Kurchatov Institute”, Moscow, 117218, Russia



(Received 22 November 2022; accepted 8 February 2023; published 27 February 2023)

The aim of this work is to generalize the method of Hubbard fields in fermion quantum Monte Carlo simulations to the case of link fields. The introduced Hubbard link fields play the role of the interaction fields responsible for the attraction and repulsion of electronic excitations at the nodes. Such improvements lead to a number of advantages concerning thermalization time, autocorrelations, metastable states, and probability distributions of the quantities. It is demonstrated that computations using five fields are more stable and reliable in the case of energy observables.

DOI: [10.1103/PhysRevE.107.025307](https://doi.org/10.1103/PhysRevE.107.025307)

I. INTRODUCTION

The Monte Carlo method of modeling quantum systems has become one of the most important tools in condensed-matter physics, nuclear physics, and high-energy physics. The method has been shown to be extremely effective in solving strong-coupling problems and for studying systems with long correlations. Nowadays, the Monte Carlo method turns out to be most popular approach available to study a large quantum system directly from the fundamental principles of quantum theory.

The study of electronic properties of graphene, as well as other semimetals, is an example of such challenges. Graphene quasiparticles are massless [1,2], so graphene physics becomes extremely nonlocal. A large effective coupling constant (with the electric field) makes it also a strongly interacting theory. Thus, the physics of electronic excitations of electron states in graphene is an important area where the Monte Carlo methods are applied.

A number of important results in graphene physics have been obtained by the Monte Carlo method: the possibility of forming an antiferromagnetic condensate [3,4], the influence of defects [5,6] and magnetic field [7–9], and the Casimir effect [10]. However, a lot of difficulties remain for applying the Monte Carlo method to fermion systems. One of the most important is the *sign problem* [11], which prevents Monte Carlo methods from being used in the important case of a nonzero chemical potential. Despite great efforts, a simple, universal and effective method to overcome the sign problem has not yet been found.

Statistical physics describes the change of a system's states through the concept of *configuration space*. In the case of graphene (as described by the extended Hubbard model's Hamiltonian), this configuration space reveals a very complex landscape, which represents another significant difficulty in connection with the Monte Carlo method. It is shown [12] that

the configuration space of the extended Hubbard model on a hexagonal lattice is a collection of valleys with a relatively low value of action S . The valleys are separated by high domain walls. A hybrid Monte Carlo process cannot leave such a valley during a finite time period after entering it. As a result, a simulation observes only some of the valleys but not the entire configuration space. To solve this problem, it is proposed [13] to introduce additional Hubbard fields in order to increase the number of degrees of freedom. In addition to the traditional Hubbard field associated with on-site interaction of charges, it was proposed to introduce a Hubbard field associated with the interaction of spins. It has been shown that such an enhancement significantly facilitates Monte Carlo simulations in the extended Hubbard model.

In the paper, it is shown that the original idea [13] can be developed further. It is proposed to consider auxiliary fields attached to *links*, and not just to nodes. In the context of Blankenbecler-Scalapino-Sugar quantum Monte Carlo (BSS QMC) [14], this technique was used, for example, in Ref. [15]. Thus, the net number of Hubbard fields in a model on a hexagonal lattice can be increased from two to five. What goals does this complication serve? First of all, this increases dimensions of the configuration space and makes it easier for the Monte Carlo process to bypass domain walls [16] in the expanded space of Hubbard fields. This helps to reduce temperatures at which the Monte Carlo simulation is efficient and relatively easy. Second, the study of complex observables associated with a large number of creation and annihilation operators becomes more accessible because a degree of divergences in statistical distribution is reduced when additional field variables are added. In this paper, we deal with energy of the electron excitations and their energy squared which contain four, six, or eight operators multiplied.

The paper is organized as follows: In Sec. II the formulas defining the model analytically are given and the procedure for introducing link fields is shown. Section III demonstrates the results of the technical tests of a computer program, which prove a correctness of simulations and the enhancement in the performance. In Sec. IV, energy-like observables are calculated within a wide range of temperatures in order to compare

*sd.mostovoy@physics.msu.ru

†pavlovsky@physics.msu.ru

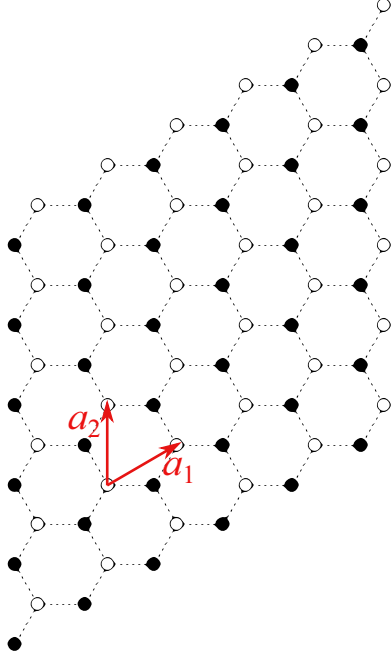


FIG. 1. A geometry of the lattice used in computations. Two primitive vectors of the lattice are shown, periodicity along which is imposed.

their features in case of two- and five-field approaches. Finally, Sec. V summarizes the results obtained and outlines the plans for further research.

II. MODEL DESCRIPTION

Let us consider an extended Hubbard model on a hexagonal lattice. A plane of $2L^2$ sites is enclosed with periodic boundary conditions of Born-von Kármán type as presented in Fig. 1. The Hamiltonian reads

$$\hat{H} = -\kappa \sum_{\langle x,y \rangle, \sigma} (\hat{a}_{x,\sigma}^\dagger \hat{a}_{y,\sigma} + \text{H.c.}) + \frac{1}{2} \sum_{x,y} V_{xy} \hat{q}_x \hat{q}_y, \quad (1)$$

where κ is the hopping parameter, $\langle x, y \rangle$ indicates adjacent sites, σ stands for a spin projection (up or down), $\hat{q}_x = \hat{a}_{x,\uparrow}^\dagger \hat{a}_{x,\uparrow} + \hat{a}_{x,\downarrow}^\dagger \hat{a}_{x,\downarrow} - 1$ defines an electric charge on a site, with $\hat{a}_{x,\sigma}$ being an annihilation operator for a σ -spin particle at node x . V_{xy} refers to a matrix of electrostatic interaction with parameters V_{00} and V_{01} depending on the distance between two electrons (on-site and nearest neighbors are involved). The dimensions of the matrix are $N_s \times N_s$, where $N_s = 2L^2$. The coefficients are chosen to be $\kappa = 2.8$ (eV), $V_{00} = 3.5\kappa$, $V_{01} = 0.8\kappa$. This set corresponds to semimetal—a complex state with a complicated configuration landscape. The calculation itself is performed by the quantum hybrid Monte Carlo method. A relevant technical description can be found in Ref. [17], and the procedure for discretizing the partition function within a path integral approach is described in detail in Ref. [13]. The total number of time slices amounts to $2N_T$, because each of N_T transitions in Euclidean time is quantized into two factors, concerning the kinetic and interaction parts of the Hamiltonian. $N_T = 60$ is used throughout the computations. Our computer code can work in a mode using two

Hubbard fields, and the computations implement the following partition function ($\beta = 1/T$, $k_B = 1$):

$$\mathcal{Z} = \text{Tr}\{e^{-\beta\hat{H}}\} = \int \mathcal{D}[\zeta, \zeta^*] \mathcal{D}[\phi, \chi] \exp\{-S_{\text{HS}} - \zeta^*(MM^\dagger)^{-1}\zeta\}, \quad (2)$$

the action of Hubbard fields is ($\delta = \beta/N_T$)

$$S_{\text{HS}} = \frac{\delta^n}{2} \phi \tilde{V}^{-1} \phi + \frac{[\chi - (1 - \alpha)V_{00}\delta^{1-m}]^2}{2(1 - \alpha)V_{00}} \delta^n, \quad (3)$$

$$\tilde{V}_{xy} = \alpha V_{00} \delta_{xy} + (1 - \delta_{xy}) V_{xy}, \quad (4)$$

where the fermionic matrix represents

$$M = \begin{bmatrix} 1 & 0 & 0 & 0 & 0 & \dots & -E_{N_T-1}^{(f)} \\ E_0^{(k)} & 1 & 0 & 0 & 0 & & 0 \\ 0 & E_0^{(f)} & 1 & 0 & 0 & & 0 \\ 0 & 0 & E_1^{(k)} & 1 & 0 & & 0 \\ 0 & 0 & 0 & E_1^{(f)} & 1 & & 0 \\ \vdots & & & & & \ddots & \vdots \\ 0 & 0 & 0 & 0 & 0 & \dots & 1 \end{bmatrix}, \quad (5)$$

$$E_t^{(k)} = -\exp \left\{ \kappa \delta \sum_{\substack{x,y \\ (a,b)}} (\delta_{ax} \delta_{by} + \delta_{ay} \delta_{bx}) \right\}, \quad (6)$$

$$E_t^{(f)} = -\text{diag} \exp \{-\delta^m (i\varphi_{xt} + \chi_{xt})\}, \quad (7)$$

where $E_t^{(f)}$ are diagonal $N_s \times N_s$ matrices with space indices x, y ; $E_t^{(k)}$ are dense $N_s \times N_s$ matrices, $\alpha = 0.95$ is a mixing parameter for Hubbard fields of φ_{xt} and χ_{xt} , and $t = 0, N_T - 1$ serves as a reference number of a time slice (with total number of $2N_T$). To derive (3) one should use the following form of the Hubbard-Stratonovich transform, with an additional parameter n which helps to control time-discretization errors (n and m are tied by $2m - n = 1$):

$$\exp \left\{ -\frac{1}{2} \hat{q} V \hat{q} \delta \right\} = \int \mathcal{D}[\varphi] \exp \left\{ -\frac{\delta^n}{2} \varphi V^{-1} \varphi - i\delta^m \varphi \hat{q} \right\}. \quad (8)$$

In the current paper, $n = -1$ will be fixed. However, a dependence of Hubbard fields' amplitudes n is an interesting question itself. We have launched our program for a set of n and have derived a conclusion that n should be chosen to be negative; however, all values from the list $-1, -2, -3$ are good enough, so the difference in results and stochastic properties of Monte Carlo time series can be a topic of further investigation. Of course, n and m are not limited to integers, so this choice is a matter of taste only.

The principal *innovation* in our work is an introduction of the auxiliary *link* fields that supplement the main φ_{xt} and χ_{xt} fields defined on the nodes. It is assumed that these additional degrees of freedom greatly increase the dimension of a configuration space, which, first, simplifies a generation of a sequence of system configurations during the Monte Carlo flow, and, second, reduces the divergences in observables consisting of a large number of creation-annihilation operators.

The second circumstance turns out to be significant due to a complicated structure of observables (products of six and eight operators) involved in our research. The problem is related to fermion matrix zeros in the configuration space of the model because a propagator corresponds to elements of the inverse fermionic matrix. The Monte Carlo flow depends on the zeros which can disturb a numeric algorithm to walk around configurations. This can impose limits on the selection of configurations. A detailed discussion can be found in Ref. [18].

Let us show how supplementary *link* fields are proposed to be introduced into the model. It is suggested that one can isolate a perfect square for the product of operators at distinct points (this is possible due to the commutation property $[\hat{q}_x, \hat{q}_y] = 0$):

$$\begin{aligned} & \frac{V_{00}}{2} \sum_x \hat{q}_x^2 + \frac{V_{01}}{2} \sum_{x \neq y} \hat{q}_x \hat{q}_y \\ &= \frac{V_{00}}{2} \sum_x \hat{q}_x^2 + \frac{V_{01}}{4} \sum_{x \neq y} ((\hat{q}_x + \hat{q}_y)^2 - \hat{q}_x^2 - \hat{q}_y^2) \\ &= \frac{V_{00}}{2} \sum_x \hat{q}_x^2 - 3 \frac{V_{01}}{2} \sum_x \hat{q}_x^2 + \frac{V_{01}}{4} \sum_{x \neq y} (\hat{q}_x + \hat{q}_y)^2 \\ &= \frac{1}{2} \sum_x V'_{00} \hat{q}_x^2 + \frac{V_{01}}{4} \sum_{x \neq y} (\hat{q}_x + \hat{q}_y)^2, \end{aligned}$$

where $V'_{00} = V_{00} - 3V_{01}$ indicates a modification of a site interaction. Within the bounds of Ref. [13] a site field will be decomposed into two components φ_{xt} and χ_{xt} in the following manner:

$$\alpha \frac{V'_{00}}{2} \sum_x \hat{q}_x^2 - (1 - \alpha) \frac{V'_{00}}{2} \sum_x \hat{s}_x^2 + (1 - \alpha) V'_{00} \sum_x \hat{s}_x,$$

where $\hat{s}_x = \hat{a}_{x,\uparrow}^\dagger \hat{a}_{x,\uparrow} - \hat{a}_{x,\downarrow}^\dagger \hat{a}_{x,\downarrow} + 1$ defines spin at a site. The procedure how the expressions of \hat{q}_x^2 and \hat{s}_x^2 can be rewritten is described in the papers mentioned above, so we pay attention to the link part only:

$$\begin{aligned} & \exp \left\{ -\delta \frac{V_{01}}{4} \sum_x (\hat{q}_x + \hat{q}_{x+\mu})^2 \right\} \\ &= \int \mathcal{D}[\xi^{(\mu)}] \exp \left\{ -\frac{\xi^{(\mu)^2}}{V_{01}} \delta^n - i \delta^m \sum_x \xi_x^{(\mu)} (\hat{q}_x + \hat{q}_{x+\mu}) \right\} \\ &= \int \mathcal{D}[\xi^{(\mu)}] \exp \left\{ -\frac{\xi^{(\mu)^2}}{V_{01}} \delta^n - i \delta^m \sum_x (\xi_x^{(\mu)} + \xi_{x-\mu}^{(\mu)}) \hat{q}_x \right\}, \end{aligned}$$

where $\mu = 1, 2, 3$ and $\xi^{(\mu)}$ is a vector composed of $\xi_x^{(\mu)}$. In the second sum of the last expression, a substitution $x + \mu \rightarrow x$ is made in order to get $\hat{q}_{x+\mu}$ in the form of \hat{q}_x . A symbol of $x - \mu$ designates a site in the direction opposite to those of μ (i.e., $y = x - \mu$ means that a neighbor of y in the direction μ is x). One can show that ξ fields are manifested in the fermion matrix in the following way:

$$E_t^{(1)} = -\text{diag} \exp \left\{ -\delta^m \left[\chi_{xt} + i \left(\varphi_{xt} + \sum_\mu \xi_{xt}^{(\mu)} + \sum_\mu \xi_{x-\mu,t}^{(\mu)} \right) \right] \right\}. \quad (9)$$

So, we have demonstrated how the dimension of the configuration space of the model can be increased to five (see Fig. 2). In this work, an attempt is made to compare the results of such “expended” calculations with standard ones in cases of order parameters and energetic quantities, so that an inaccuracy in values obtained can be reduced. One should expect to observe the difference between results obtained with two and five fields because additional degrees of freedom may make Monte Carlo configurations more chaotic and

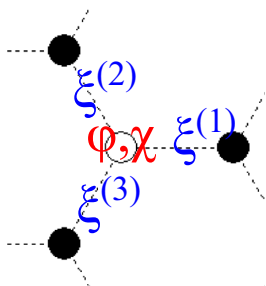


FIG. 2. Five fields used in our research: two site fields φ_{xt} and χ_{xt} on each site x together with link fields $\xi_{xt}^{(\mu)}$, $\mu = \overline{1, 3}$ attached to links.

independent. Moreover, features of observables’ distributions [16] in the configuration space are affected. The data presented below will show that this is the case. The second opportunity, the selection of n , manages the amplitude of the fields. The consequences of this will be studied in subsequent work.

One can note that $V'_{00} = V_{00} - 3V_{01}$ has appeared in the formulas. The fact that a set of points $(V_{00}, V_{00}/3)$ on a phase diagram of the model represents the boundary of the area available to this method of calculations is known [19] but in the case of two fields is “hidden” in the structure of eigenvalues of \tilde{V}^{-1} . In our case (five fields) it becomes explicit and obvious. This can be regarded as a beautiful touch of the five-field formalism.

It is well known that a long-range potential plays some nontrivial role in graphene [20]. It is worth saying that the method by which supplementary link fields are introduced does not preclude including further interaction radii into V_{xy} such as V_{02} or V_{03} [21].

III. TECHNICAL PROPERTIES

To verify how supplementary link fields influence a configuration space landscape one can observe an evolution of

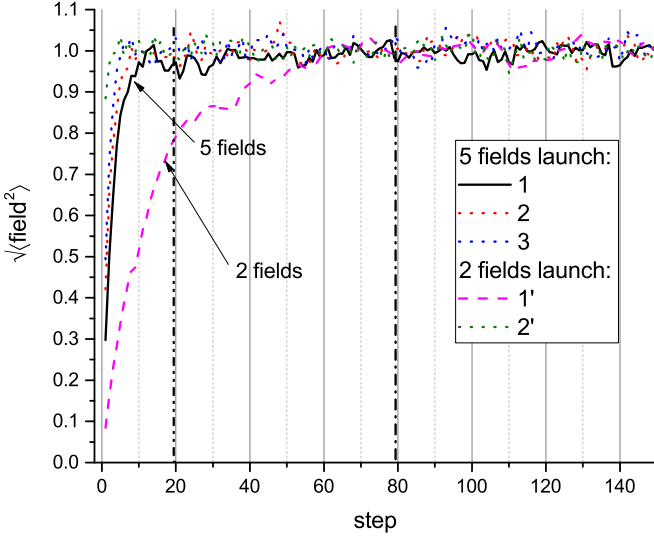


FIG. 3. An example of the fields' evolution obtained in two program launches for lattice 6×6 . Mean-square fields are shown. Labels 1, 2, and 3 refer to φ_{xt} , χ_{xt} , and $\xi_{xt}^{(2)}$ for a five-field launch while labels 1' and 2' mean φ_{xt} and χ_{xt} for a two-field mode. Values are normalized by a value at step 150. It took four times longer for the two-field launch to reach representative configuration states in comparison with the five-field case (the marks are shown as dash-dot and dash-dot-dot, respectively).

φ_{xt} , χ_{xt} , and $\xi_{xt}^{(\mu)}$ during a thermalization process. After some program launches were performed, it turned out that significantly fewer algorithm steps are needed to reach a region of well-thermalized configurations (this was tested by analyzing moving averages of fields, the action S and the autocorrelation times of several observables) when using five fields in comparison with the two-field case. A moving average of M successive computations of an observable x during a Monte Carlo series is defined as follows:

$$\frac{1}{M} \sum_{i=1}^M x_i.$$

In the course of the work, the measurement number M required to stabilize this value was estimated.

An example of a simulation program launch is shown in Fig. 3. Thus, most likely, the technical gain in thermalization itself is achieved by reducing the number of steps required to obtain “typical” field values for given model parameters. Moreover, a five-field approach does not require to find a reverse of the interaction matrix V_{xy} which also simplifies coding and debugging (the operation occurs four times in the course of the algorithm). The calculation of additional fields (involves the molecular dynamics evolution and the action S) does not increase the work time by more than 4.4%. Taking into account that the number of algorithm steps is reduced by 10–20 times (due to the need for fewer configurations: to obtain a comparable quality of statistics, it became possible to take 1500 measurements instead of 10 000; moreover, one can use every generated configuration without skipping a few), it is possible to obtain a significant benefit when obtaining a

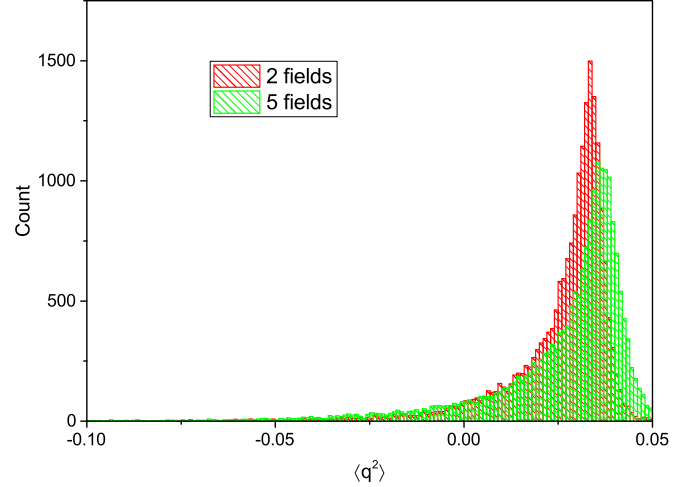


FIG. 4. A distribution of $\langle q^2 \rangle$ (per sublattice). It is suggested that, in the case of five fields, a Monte Carlo process involves more distinct values of the observable, so it covers a wider region of a configuration space. The peak is more smooth and slopes grow more gentle. A fitting problem of the probability distribution is discussed in Sec. IV. Computation for 6×6 and $T = 0.3\kappa$. Sample size is 20 000.

series of statistical data to determine the average values of the observables.

An important conclusion shall be drawn: a comparison of the thermalization curves shows that the introduction of five fields significantly reduces the thermalization time by several times, which increases the effectiveness and performance of the Hybrid Monte Carlo.

The fluctuations sharing between link fields (according to their mathematical definition) seem to be another positive factor. This can help the Markov chain Monte Carlo simulation to observe a configuration space in a flexible manner while generating new configurations. It can be visualized by collecting sequential values of a quantity during a Monte Carlo simulation in order to build a histogram. If one performs this concerning mean of charge squared per sublattice:

$$\langle q^2 \rangle = \frac{1}{2} \left\{ \frac{1}{L^4} \left\langle \left(\sum_{x \in A} \hat{q}_x \right)^2 \right\rangle + \frac{1}{L^4} \left\langle \left(\sum_{x \in B} \hat{q}_x \right)^2 \right\rangle \right\}, \quad (10)$$

the result argues that the distribution falls smoother in case of five fields and that a larger range of values are presented in the vicinity of the modal (most probable) value (see Fig. 4). The curve itself is reduced in height and more resembles a Gaussian when five fields are used. The expectation values remain unchanged though. A long so-called heavy tail is manifested in both the cases, but a numerical comparison of a goodness of the distribution form reveals a difference between two- and five-field results and is discussed for all the observables under the study in the next section.

A technical feature that differs the usage of two and five fields should be mentioned. It turned out that the integration step $\Delta\tau$ of the molecular dynamics (an essential part of hybrid Monte Carlo that obtains “new” configurations) varies with temperature in case of five fields if one wants to keep acceptance rates as high as 95%–98%. Specifically, in the

TABLE I. Autocorrelation times as a function of temperature in the case of two- and five-field approaches.

T/κ	Two fields	Five fields
0.1	5.6	0.8
0.15	5.2	1.2
0.2	4.6	1.0
0.25	4.0	0.9
0.3	3.6	0.8
0.4	2.1	1.0
0.5	1.8	1.1
0.6	1.5	1.2
0.7	1.7	1.0
0.8	1.6	1.1

range of $0.06 < T/\kappa < 0.1$, $\Delta\tau = 0.009$ was used with both two and five fields while it required 0.008 at $T = 0.3\kappa$ and 0.005 at $T = 0.6\kappa$ with five fields. Actually, this tuning did not cause a problem at all, but noticeably more independent configurations are obtained, which becomes an advantage of the five-field approach. This can be proved by calculating the so-called *autocorrelation times* [22] for Monte Carlo time series. The results of one such investigation are shown in Table I (for energy-like observables, for $\langle q^2 \rangle$ the times are less, but still exceed the best values for five fields by 2.1–2.8 times).

An important circumstance is the advantage of the five-field method in a physically interesting temperature range, because it is necessary to perform calculations at low temperatures. It can be expected that the advantage will remain at lower temperatures due to the small temperature dependence of the data for five fields, evident from the table. Besides, one can see that, in the two-field approach, the temperature dependence is significant, so it takes more effort to maintain acceptable statistics while using two fields in comparison with the five-field technique.

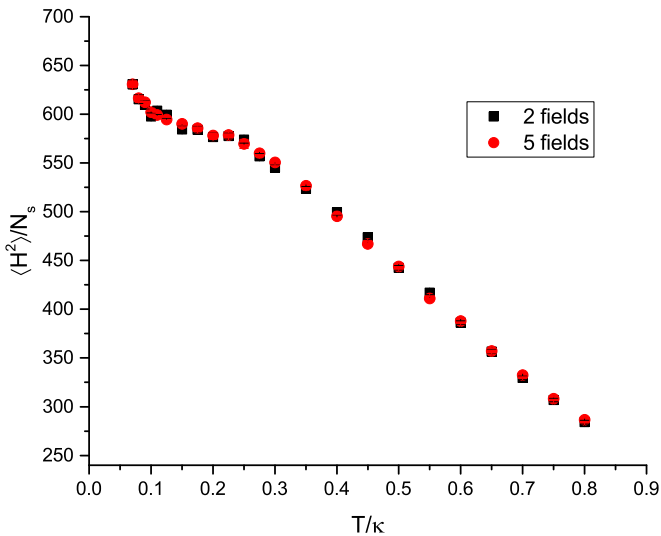


FIG. 5. $\langle \hat{H}^2 \rangle$ (per site) for lattice 6×6 as a decreasing function of temperature. 6×6 lattice. This feature arises due to a contribution of last two terms in (11).

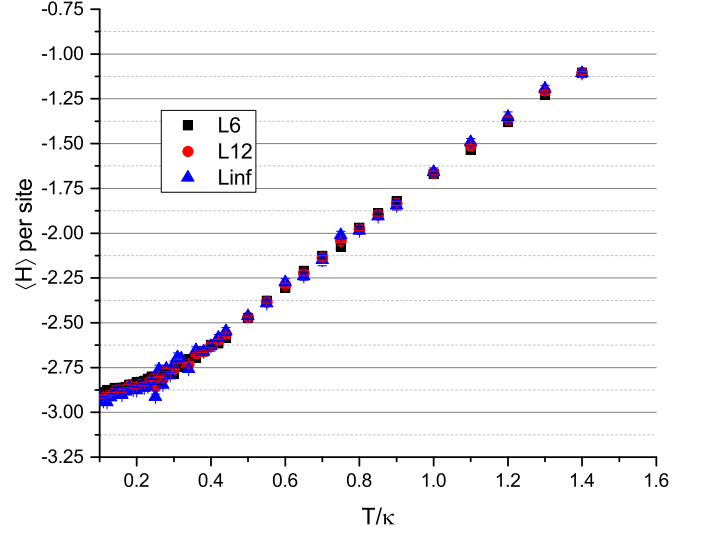


FIG. 6. A “volume effect” test. Mean energy is computed for a large temperature range for $L = 6$ and $L = 12$. An infinite-volume limit is shown (labeled as “Linf”). One can see that the difference is negligible within statistical errors.

The times can be reduced by increasing $\Delta\tau$, a step of the molecular dynamics, but this has a limit because the acceptance rate lowers. Another approach is to skip several intermediate configurations between sequential “measurements,” but the strategy is less time efficient. Thus, it is argued that fields can help to produce Monte Carlo series of a better quality.

IV. TRIALS OF ENERGY COMPONENTS

Let us present the results of further tests in favor of Monte Carlo simulations using three additional Hubbard fields $\xi_{xt}^{(\mu)}$. As mentioned above, one of the consequences of expanding

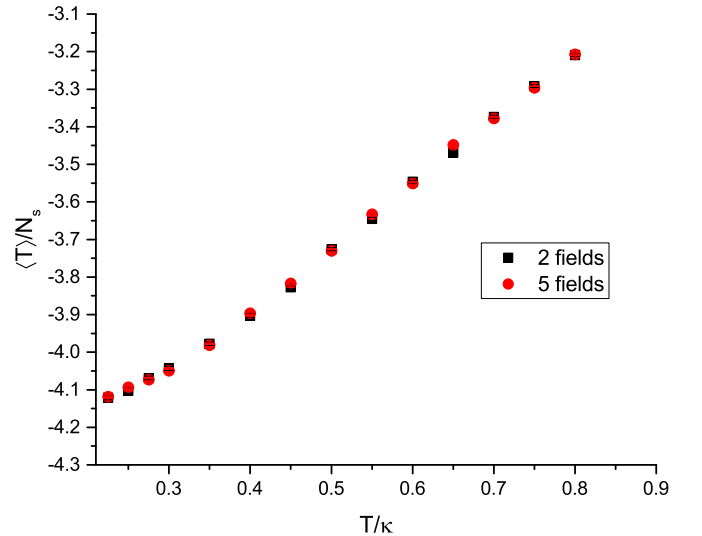


FIG. 7. Comparison of kinetic term thermal behavior for two-field and five-field approaches. As $\langle \hat{T} \rangle$ has the simplest structure possible, everything looks reliable.

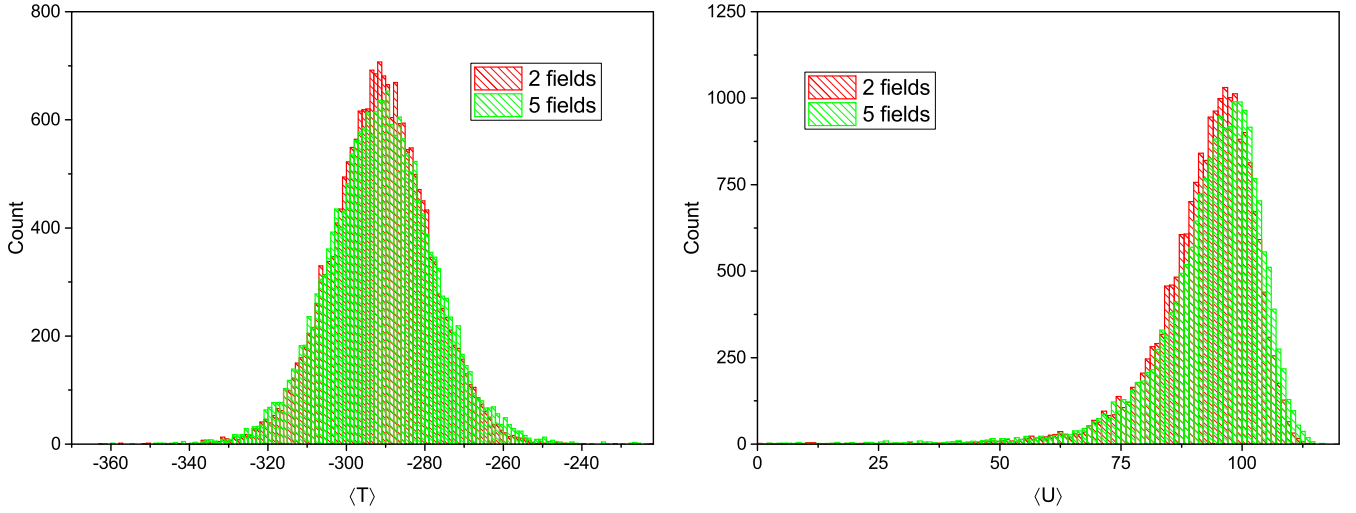


FIG. 8. The histograms help to compare features of kinetic and potential energies from a point of view of values presented in distributions obtained for 6×6 . One can see that, while $\langle T \rangle$ is obvious of a Gaussian form, $\langle U \rangle$ reveals exponential suppression on the right but has a long tail in the opposite direction. The latter can cause problems with higher distribution function moments, so it is desirable that a contribution of the tail is reduced. Five fields are helpful in this.

the configuration space is a modification of distributions of observables. To check how well this works a number of physical quantities in the form of creation-annihilation operator combinations were computed and statistics of 20 000 numbers was investigated. One of meaningful physical quantities with a large number of operators multiplied is the square of the Hamiltonian $\langle \hat{H}^2 \rangle$ which contains products of 8, 6, 4, and 2 operators. The exact expression of $\langle \hat{H}^2 \rangle$ is outlined in Appendix.

To begin with, one should respect an operator character of the $\langle \hat{H} \rangle$ and compute the Hamiltonian squared in a proper way. Indeed,

$$\begin{aligned} \langle \hat{H}^2 \rangle &= \langle (\hat{T} + \hat{U})^2 \rangle = \langle \hat{T}^2 \rangle + \langle \hat{U}^2 \rangle + \langle \hat{T}\hat{U} \rangle + \langle \hat{U}\hat{T} \rangle \\ &\neq \langle \hat{T} + \hat{U} \rangle^2 = (\langle \hat{T} \rangle + \langle \hat{U} \rangle)^2, \end{aligned} \quad (11)$$

and $\langle \hat{T}\hat{U} \rangle + \langle \hat{U}\hat{T} \rangle \neq 2\langle \hat{T} \rangle \langle \hat{U} \rangle$. One consequence of (11) is a *descending* behavior of $\langle \hat{H}^2 \rangle$ with temperature rising (see Fig. 5). One can treat $\langle \hat{T}\hat{U} \rangle$ as $\sum_m \langle \hat{T} | m \rangle \langle m | \hat{U} \rangle$, where $\{|m\rangle\}$ is a complete set of states. Simulations show that the multipliers have different signs, so this item *reduces* the sum composing $\langle \hat{H}^2 \rangle$. There is no doubt that the square of the energy $\langle \hat{H} \rangle$ itself is an increasing function of temperature, as an energy does (see Fig. 6).

Second, in numerical computations on the lattice, a “volume effect” should be checked to be sure of the correctness of the results. This means that when the size of the problem increases, the magnitude of the quantities obtained should not change significantly. Let us demonstrate that this is the case in our calculations of energy observables. Figure 6 presents computation results of $\langle \hat{H} \rangle$ (per site) in case of 6×6 , 12×12 lattices and extrapolations (point-wise) to the infinite-lattice limit. A negligible volume effect with respect to energy quantities can be assured. Note that such observables as $\langle S_z^2 \rangle$ (S_z is the z component of a spin, the expression has a form of (10)

with

$$\hat{S}_{z,x} = \frac{1}{2}(\hat{a}_{x,\uparrow}^\dagger \hat{a}_{x,\uparrow} - \hat{a}_{x,\downarrow}^\dagger \hat{a}_{x,\downarrow})$$

substituted) and $\langle q^2 \rangle$ suffer from the severe volume effect (see, for example, Ref. [13]). Now, one can conclude that it is safe to perform energy computations with $L = 6$ which requires significantly less CPU time.

This is why we continue by presenting results for $L = 6$ ($L = 12$ was checked at a few temperatures, of course, the volume effect proved to be small enough).

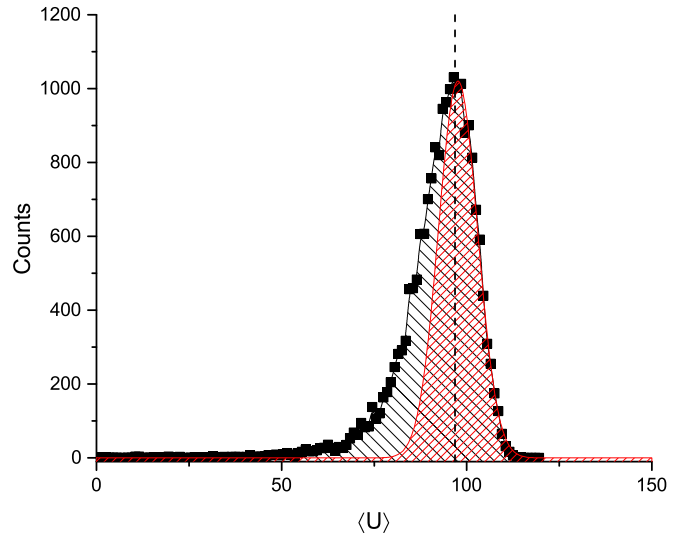


FIG. 9. A visualization of the method proposed to compare contributions of a heavy tail to the net probabilities. A red curve and crossed hatch is the Gaussian fitting of the right side of the data (black points). The single hatch fills an area under the curve of the real distribution. Regions to the left of a dashed line are used to find a fraction of non-Gaussian contributions. An example of two fields is a 6×6 lattice. See description in the main text.

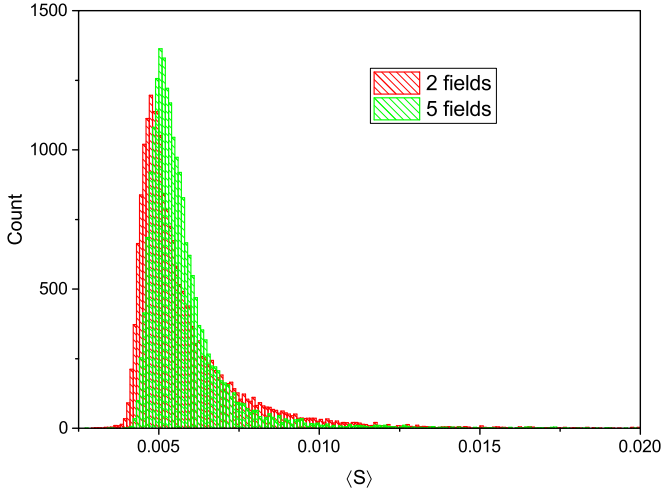


FIG. 10. A histogram of values of $\langle S_z^2 \rangle$. In the case of five fields the tail is obviously lower.

The results for kinetic term of the Hamiltonian are presented in Fig. 7. The initial expression reads

$$\langle \hat{T} \rangle = -\kappa \sum_{\langle x,y \rangle, \sigma} \langle \hat{a}_{x,\sigma}^\dagger \hat{a}_{y,\sigma} + \hat{a}_{y,\sigma}^\dagger \hat{a}_{x,\sigma} \rangle$$

and contains products of two operators only, so no mathematical difficulties arise. The graph confirms that everything goes well.

Next, one turns to a potential term

$$\langle \hat{U} \rangle = \langle \hat{U}_1 + \hat{U}_2 \rangle = \frac{1}{2} \sum_{x,y} v_{xy} \langle \hat{q}_x \hat{q}_y \rangle,$$

containing products of four operators. U_1 includes on-site interactions of electrons at the same site ($x = y$) while U_2 designates nearest-neighbor interactions. From this point on, some problems arise. Figure 8 presents the difference between statistical distributions of $\langle \hat{T} \rangle$ and $\langle \hat{U} \rangle$ for a launch of 20 000 computations of observables. One can see that configurations

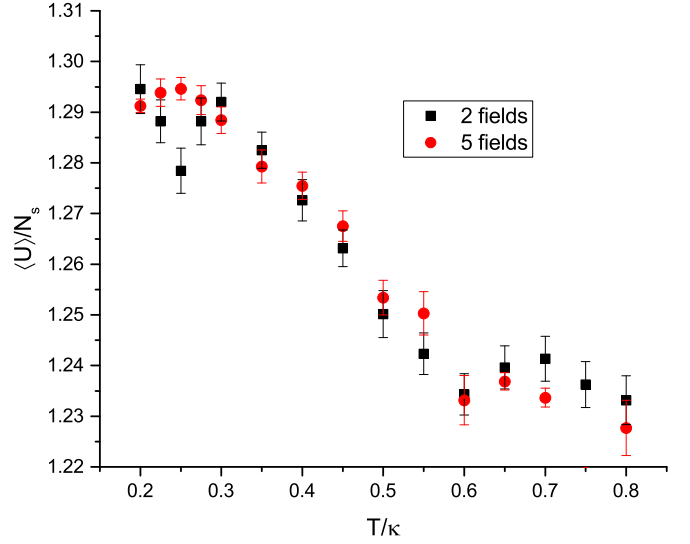


FIG. 12. A comparison of the interaction term thermal behavior for two-field and five-field approaches. Indications to metastable states are noticeable in case of two fields at $0.2 \lesssim T/\kappa \lesssim 0.3$. An observed noise is permitted due to a complicated physical character of a semimetal state of the Hubbard model in the vicinity of $U = 3.2$, $V = 0.8$. The five-field approach still yields a more stable result.

with increased interaction energy are depressed exponentially while there are configurations with moderate and weak values of $\langle \hat{U} \rangle$. Nothing of the kind takes place as to $\langle \hat{T} \rangle$. Almost a perfect Gaussian form occurs in the latter case. $\langle \hat{U} \rangle$ reveals a so-called heavy-tailed distribution when one of its slopes falls slower than an exponent does. As a result an attempt to compute higher-distribution moments such as a variance can run into some difficulties [16]. So, let us inspect if the five-field approach can help to enhance the form of the distribution of the observables.

It is proposed to compare the contributions of heavy tails as follows: In Fig. 8 the right-hand side of the $\langle \hat{U} \rangle$ distribution resembles a Gaussian, and a fitting confirms this hypothesis.

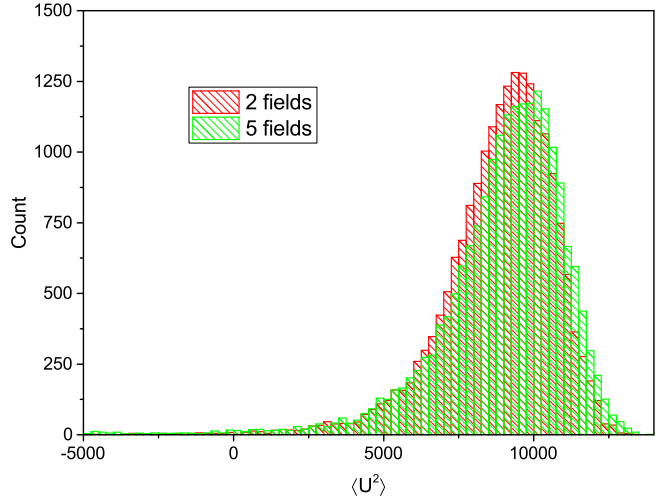
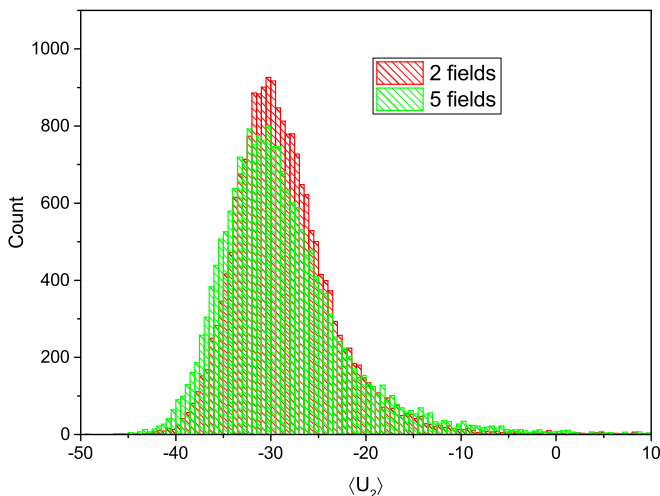


FIG. 11. A histogram of values of $\langle \hat{U}_2 \rangle$ and $\langle \hat{U}^2 \rangle$. The five-field result is more like a Gaussian and calculations yield that a long tail is somewhat better in this case.

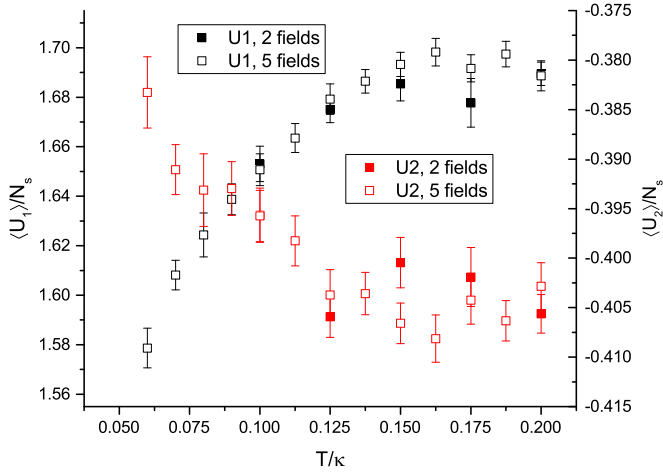


FIG. 13. Two components of the potential energy $\langle \hat{U} \rangle$ per site in 6×6 lattice for low temperatures. While results for two-fields fluctuate substantially, the five-field approach stabilizes the computations so that a smooth curve can be traced within statistical error bars.

So, one can imagine a perfect symmetrical distribution with the center at point where real distribution maximum exists but of a Gaussian width obtained by fitting the right-hand side. For our example, a relative statistical error of the width evaluation is around 3% only. Next, one computes numerically the area A restricted by the heavy-tailed side (in our case it is the left-hand one) and subtracts the corresponding area of the Gaussian curve. Finally, divide the value by A to estimate how much of the distribution exceeds the desired (Gaussian) curve (see Fig. 9). In the case of $\langle \hat{U} \rangle$ the quantity computed equals 39.48% for two fields and 33.68% for five fields. So, the tendency is rather encouraging.

Actually, for all the observables from the list— $\langle S_z^2 \rangle$, $\langle q^2 \rangle$, $\langle T \rangle$, $\langle U \rangle$, $\langle U_1 \rangle$, $\langle U_2 \rangle$, $\langle \hat{H} \rangle$, $\langle \hat{H}^2 \rangle$ —an area excess of the distribution over the Gaussian (found in the way mentioned above) is reduced when using five fields in comparison to a two-field approach. The most prominent example is of $\langle q^2 \rangle$: 40.7% for two fields and 26.6% for five fields. The examples are presented in Figs. 4, 10, and 11. The most complex combinations of multiple (up to eight) creation-annihilation operators considered in the paper ($\langle \hat{U} \hat{U} \rangle$) are also improved. The change for $\langle \hat{U} \hat{U} \rangle$ is from 39.19% to 36.46%.

To demonstrate how the modification affects the simulation results, let us look closely at the potential energy (Fig. 12) and its components (Fig. 13) at low temperatures. The values obtained in the five-field approach seem to be located smoother so that one can connect them with a continuous curve without violating the restrictions of statistical error bars. On the contrary, the results for two fields reveal an indication of metastable states, so that it requires several independent runs of a program to estimate the mean and standard deviation reasonably. Although the results do follow the same behavior, the stability of the numerical results is essential in connection with a forthcoming calculation of derivatives of the (numerical) function or differences of large values. This takes place in the context of a heat capacity (defined both by a derivative and via energy variance), for example. So, due to the fact that five fields help walking through a configuration space in a more flexible and gentle manner, which is supported

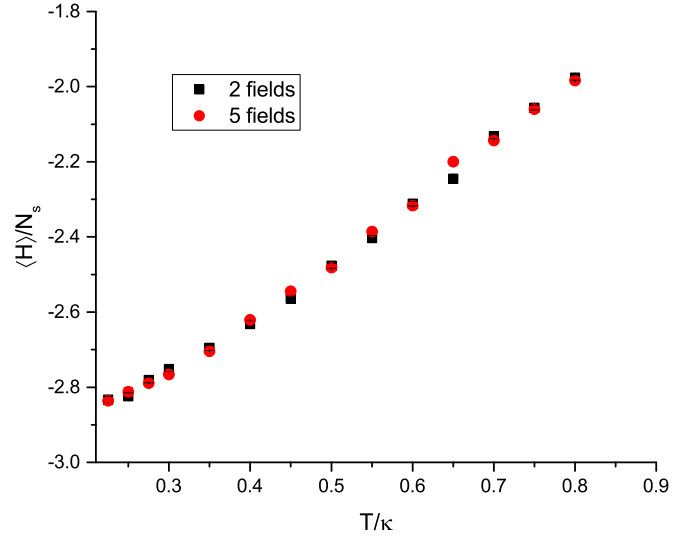


FIG. 14. Thermal behavior of $\langle \hat{H} \rangle$ (per site) for 6×6 in launches with two and five fields. The results are consistent.

by the data presented above, the distributions are modified with additional contributions from wide regions of a configuration space which make them more reliable for sequential calculations.

If $\langle \hat{H} \rangle = \langle \hat{T} \rangle + \langle \hat{U} \rangle$ is computed, the overall result can be outlined as follows (Fig. 14): A regular kinetic part (with high agreement between two-field and five-field approaches) is superposed with a fluctuating potential part (with some deviations between the two cases). Actually, this *can influence* the heat capacity determined by a derivative ($\partial \mathcal{E} / \partial T$, $\mathcal{E} = \langle \hat{H} \rangle$) for example, but appropriate fitting of the $\mathcal{E}(T)$ curve serves as a good remedy. On the other hand, as stated above, five-field launches seem to produce more stabilized values, so the fitting may have better quality.

It is time to check $\langle \hat{H}^2 \rangle$. Let us do this by plotting a histogram of $\langle \hat{H}^2 \rangle$ values for two-field and five-field simulations (Fig. 15). It is noticeable that, in the latter case, a distribution is more regular at its top and has smoother side falls. There are more configurations with values of $\langle \hat{H}^2 \rangle \approx 22\,000$ (eV²). It should be noted that these features do not vanish when temperature rises, which is the case for $\langle \hat{T} \rangle$ and $\langle \hat{U} \rangle$, so the effect remains stable. This shows the difference between four and eight or six operators multiplied. The distributions were tested at $T = 0.3\kappa$ and $T = 0.6\kappa$. An effect of a distribution refinement on the final results of $\langle \hat{H}^2 \rangle$ is depicted in Fig. 16. Points corresponding to a five-field launch fluctuate less intensively and the change of $\langle \hat{H}^2 \rangle(T)$ around $T = 0.2\kappa$ is more apparent.

It is proposed to put these *mathematical* observations into practice by applying them to a heat-capacity computation. We have run into a number of nontrivial features while investigating C as a function of temperature, which are caused by complicated rearrangements in electron spatial density. For example, two phase transitions at $T = 0.028\kappa$ and 0.075κ are guessed with $V_{00} = 3.2\kappa$ and $V_{01} = 0.8\kappa$. Presumably they are related to formation and melting of an exciton condensate. The particular results obtained will be a topic of a separate paper.

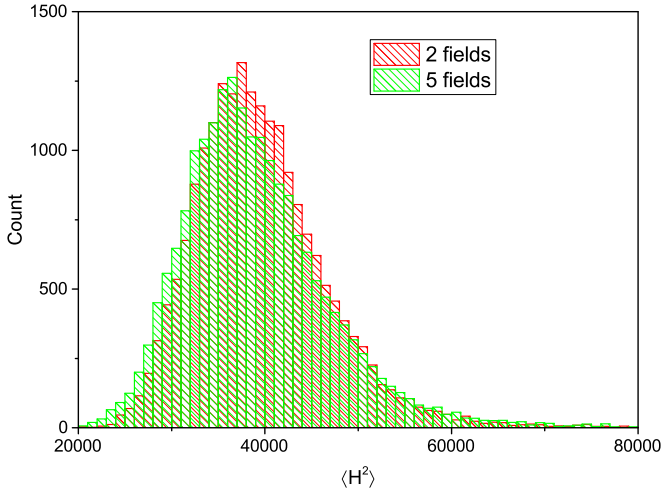


FIG. 15. A histogram of $\langle \hat{H}^2 \rangle$. An analysis showed that an excess of nonexponential tail above the Gaussian fitting obtained from a good (left) part is reduced from 30.57% to 28.78% when involving five fields.

V. CONCLUSION

The aim of our work was to generalize the method of Hubbard fields in fermion Monte Carlo simulation to the case of link fields. Such an improvement looks self-consistent from a physical point of view. The introduced Hubbard link fields play a role of the interaction fields responsible for the attraction and repulsion of electronic excitations at the nodes. In the paper we aim to show that the extension of the configuration space also helps hybrid Monte Carlo simulations due to improving the complex landscape of the extended Hubbard model that makes it difficult to bypass domain walls.

Collecting the advantage which link Hubbard fields yield, one can state the following:

- (1) Thermalization time is reduced by several times.
- (2) Autocorrelation time is also reduced, especially in the region of low temperatures, where physical results are attractive.
- (3) Fluctuation properties of observables are refined.
- (4) Metastable states are depressed, they occur less frequently.
- (5) An analytical form of action to compute using a computer is simplified; moreover, the existence of the boundary $V_{01} = U_{00}/3$ becomes explicit.
- (6) Heavy tails of distributions represent a smaller contribution to the whole probability.

In this work, we calculated the principle ingredients of the heat capacity of the gas of electron excitations in the extended Hubbard model on a hexagonal lattice. The results for C itself and extensive analysis of its behavior in vast range of temperatures will be presented in the next presentation.

It worth saying that the development proposed does not solve the problem of domain walls completely, but it helps Monte Carlo to observe a configuration space in a better way in comparison to the standard case. The statement can be proved by histogram examination which provides evidence for better distribution quality. Autocorrelation times are reduced and metastable states seem to emerge less often while using the five-field approach.

ACKNOWLEDGMENTS

The work was supported by grant from the Russian Science Foundation (project number 21-12-00237). The research is carried out using the equipment of the shared research facilities of HPC computing resources at Lomonosov Moscow State University [23] and Institute for Nuclear Research of the Russian Academy of Sciences. We would like to express our deepest appreciation to Dr. M. Ulybyshev for valuable discussions and guiding ideas that made this study possible. We are very grateful to the referee for the careful reading of the paper and express our thanks for valuable advice and recommendations, which made it possible to improve the presentation of the content of the paper.

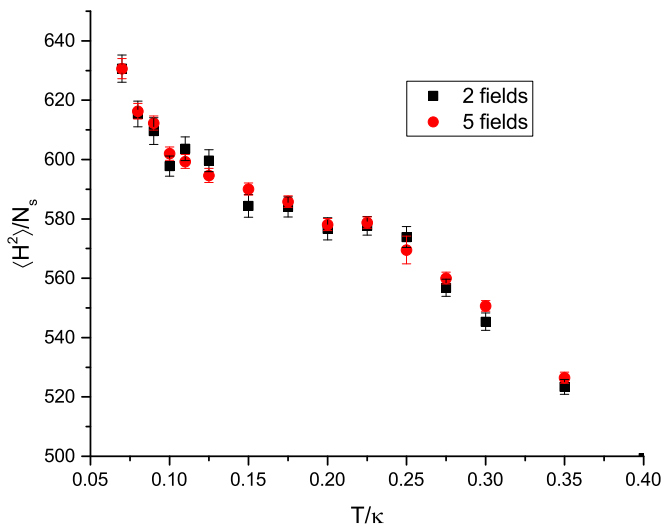


FIG. 16. $\langle \hat{H}^2 \rangle$ (per site) for lattice 6×6 in the cases of two and five fields applied. One can see a stable trend of a curve in the latter case. It improves a quality of fittings and assist processing the results when using $\langle \hat{H}^2 \rangle$ as a part of a complex mathematical expression. This is a part of Fig. 5 for low temperatures.

APPENDIX: FORM OF THE ENERGY-SQUARED MEAN

An exact expression of energy squared in terms of the fermion matrix (5):

$$\begin{aligned}
 \langle \hat{H}^2 \rangle = 2\Re \left\{ \kappa^2 \sum_{x,\mu,z,v} (P(w, y, x, z) + \delta_{w,x} M_{yz}^{-1} + M_{yx}^{-1} M_{wz}^{-1*}) \right. \\
 - \kappa \sum_{x,\mu,z,v'} V_{v'} (2P(w, y, z, w, x, z) + \delta_{w,x} P(y, z, w, z) + 2\delta_{w,z} P(w, y, w, x) - 2P(y, z, x, z) M_{ww}^{-1*} + \delta_{x,z} P(w, y, w, x) \\
 - \delta_{w,x} \delta_{x,z} M_{yw}^{-1} + \delta_{x,z} M_{yx}^{-1} M_{ww}^{-1*} - 2P(w, y, w, x) M_{zz}^{-1*} + \delta_{w,x} M_{yw}^{-1} M_{zz}^{-1*} + 2M_{yx}^{-1} P^*(w, z, w, z) - 2\delta_{w,z} M_{yx}^{-1} M_{ww}^{-1*} \\
 + \delta_{w,y} P(w, z, x, z) + \delta_{y,z} P(w, y, w, x) - \delta_{w,y} \delta_{w,z} M_{wx}^{-1} + \delta_{y,z} M_{yx}^{-1} M_{ww}^{-1*} + \delta_{w,y} M_{zz}^{-1} M_{wx}^{-1*}) \\
 + \sum_{x,\mu',z,v'} V_{\mu'} V_{v'} (P(w, x, y, z, w, x, y, z) - \delta_{w,x} P(w, y, z, w, y, z) - \delta_{w,y} P(w, x, z, w, x, z) - \delta_{w,z} P(w, x, y, w, x, y) \\
 + P(x, y, z, x, y, z) M_{ww}^{-1*} - \delta_{x,z} P(w, x, y, w, x, y) - \delta_{w,x} \delta_{x,z} P(w, y, w, y) - \delta_{w,y} \delta_{x,z} P(w, x, w, x) \\
 + \delta_{x,z} P(x, y, x, y) M_{ww}^{-1*} - \delta_{y,z} P(w, x, y, w, x, y) - \delta_{w,x} \delta_{y,z} P(w, y, w, y) - \delta_{w,y} \delta_{y,z} P(w, x, w, x) \\
 + \delta_{y,z} P(x, y, x, y) M_{ww}^{-1*} + P(w, x, y, w, x, y) M_{zz}^{-1*} + \delta_{w,x} P(w, y, w, y) M_{zz}^{-1*} + \delta_{w,y} P(w, x, w, x) M_{zz}^{-1*} \\
 + P(x, y, x, y) P^*(w, z, w, z) - \delta_{w,z} P(x, y, x, y) M_{ww}^{-1*} - \delta_{x,y} P(w, x, z, w, x, z) - \delta_{w,x} \delta_{x,y} P(w, z, w, z) \\
 - \delta_{w,z} \delta_{x,y} P(w, x, w, x) + \delta_{x,y} P(x, z, x, z) M_{ww}^{-1*} - \delta_{x,y} \delta_{x,z} P(w, x, w, x) + \delta_{w,x} \delta_{x,y} \delta_{x,z} M_{ww}^{-1} \\
 - \delta_{x,y} \delta_{x,z} M_{xx}^{-1} M_{ww}^{-1*} + \delta_{x,y} P(w, x, w, x) M_{zz}^{-1*} - \delta_{w,x} \delta_{x,y} M_{ww}^{-1} M_{zz}^{-1*} - \delta_{x,y} M_{xx}^{-1} P^*(w, z, w, z) + \delta_{w,z} \delta_{x,y} M_{xx}^{-1} M_{ww}^{-1*} \\
 + P(w, x, z, w, x, z) M_{yy}^{-1} + \delta_{w,x} P(w, z, w, z) M_{yy}^{-1*} + \delta_{w,z} P(w, x, w, x) M_{yy}^{-1} + P(x, z, x, z) P^*(w, y, w, y) \\
 - \delta_{w,y} P(x, z, x, z) M_{ww}^{-1*} + \delta_{x,z} P(w, x, w, x) M_{yy}^{-1*} - \delta_{w,x} \delta_{x,z} M_{ww}^{-1} M_{yy}^{-1*} - \delta_{x,z} M_{xx}^{-1} P^*(w, y, w, y) + \delta_{w,y} \delta_{x,z} M_{xx}^{-1} M_{ww}^{-1*} \\
 + P(w, x, w, x) P^*(y, z, y, z) - \delta_{w,x} M_{ww}^{-1} P^*(y, z, y, z) + M_{xx}^{-1} P^*(w, y, z, w, y, z) + \delta_{w,y} M_{xx}^{-1} P^*(w, z, w, z) \\
 \left. + \delta_{w,z} M_{xx}^{-1} P^*(w, y, w, y) - \delta_{y,z} P(w, x, w, x) M_{yy}^{-1} + \delta_{w,x} \delta_{y,z} M_{ww}^{-1} M_{yy}^{-1*} + \delta_{y,z} M_{xx}^{-1} P^*(w, y, w, y) - \delta_{w,y} \delta_{y,z} M_{xx}^{-1} M_{ww}^{-1*} \right\},
 \end{aligned}$$

where V_μ equals $V_{00}/2$ if $\mu = 0$ (so y is x) and $V_{01}/2$ if $\mu = 1, 2, 3$ (y is a neighbor of x), $\mu = \overline{1, 3}$, $\mu' = \overline{0, 3}$, y is found from x and μ and w is found from z and v . Pairings are defined as follows:

$$P(x, y, z, w) = M_{yz}^{-1} M_{xw}^{-1} - M_{xz}^{-1} M_{yw}^{-1},$$

$$P(x, y, z, w, u, v) = M_{xv}^{-1} P(y, z, w, u) - M_{xu}^{-1} P(y, z, w, v) + M_{xw}^{-1} P(y, z, u, v),$$

$$P(x, y, z, w, u, v, t, s) = M_{xs}^{-1} P(y, z, w, u, v, t) - M_{xt}^{-1} P(y, z, w, u, v, s) + M_{xv}^{-1} P(y, z, w, u, t, s) - M_{xu}^{-1} P(y, z, w, v, t, s).$$

-
- [1] P. R. Wallace, The band theory of graphite, *Phys. Rev.* **71**, 622 (1947).
- [2] M. I. Katsnelson, *Graphene: Carbon in Two Dimensions* (Cambridge University Press, 2012).
- [3] P. V. Buividovich, E. V. Luschevskaya, O. V. Pavlovsky, M. I. Polikarpov, and M. V. Ulybyshev, Numerical study of the conductivity of graphene monolayer within the effective field theory approach, *Phys. Rev. B* **86**, 045107 (2012).
- [4] M. V. Ulybyshev, P. V. Buividovich, M. I. Katsnelson, and M. I. Polikarpov, Monte Carlo Study of the Semimetal-Insulator Phase Transition in Monolayer Graphene with a Realistic Interelectron Interaction Potential, *Phys. Rev. Lett.* **111**, 056801 (2013).
- [5] S. N. Valgushev, E. V. Luschevskaya, O. V. Pavlovsky, M. I. Polikarpov, and M. V. Ulybyshev, Influence of defects on the conductivity of graphene within the effective theory approach, *JETP Lett.* **98**, 389 (2013).
- [6] M. V. Ulybyshev and M. I. Katsnelson, Magnetism and Interaction-Induced Gap Opening in Graphene with Vacancies or Hydrogen Adatoms: Quantum Monte Carlo Study, *Phys. Rev. Lett.* **114**, 246801 (2015).
- [7] V. V. Braguta, S. N. Valgushev, O. V. Pavlovsky, M. I. Polikarpov, and M. V. Ulybyshev, Numerical simulation of graphene in a magnetic field within the effective field theory, *JETP Lett.* **97**, 517 (2013).
- [8] V. Braguta, M. N. Chernodub, K. Landsteiner, M. I. Polikarpov, and M. V. Ulybyshev, Numerical evidence of the axial magnetic effect, *Phys. Rev. D* **88**, 071501(R) (2013).
- [9] D. L. Boyda, V. V. Braguta, S. N. Valgushev, M. I. Polikarpov, and M. V. Ulybyshev, Numerical simulation of graphene in an external magnetic field, *Phys. Rev. B* **89**, 245404 (2014).
- [10] P. Buividovich, D. Smith, M. Ulybyshev, and L. von Smekal, Interelectron interactions and the RKKY potential between H adatoms in graphene, *Phys. Rev. B* **96**, 165411 (2017).

- [11] M. Körner, K. Langfeld, D. Smith, and L. von Smekal, Density of states approach to the hexagonal Hubbard model at finite density, *Phys. Rev. D* **102**, 054502 (2020).
- [12] M. Ulybyshev, Ch. Winterowd, and S. Zafeiropoulos, Lefschetz thimbles decomposition for the Hubbard model on the hexagonal lattice, *Phys. Rev. D* **101**, 014508 (2020).
- [13] P. Buividovich, D. Smith, M. Ulybyshev, and L. von Smekal, Hybrid Monte Carlo study of competing order in the extended fermionic Hubbard model on the hexagonal lattice, *Phys. Rev. B* **98**, 235129 (2018).
- [14] R. Blankenbecler, D. J. Scalapino, and R. L. Sugar, Monte Carlo calculations of coupled boson-fermion systems. I, *Phys. Rev. D: Part. Fields* **24**, 2278 (1981).
- [15] M. Shaw and W. P. Su, Phase separation due to nearest neighbor attractive interactions in a two-dimensional model, *Mod. Phys. Lett. B* **17**, 853 (2003).
- [16] M. Ulybyshev and F. Assaad, Mitigating spikes in fermion Monte Carlo methods by reshuffling measurements, *Phys. Rev. E* **106**, 025318 (2022).
- [17] D. Smith and L. Von Smekal, Monte Carlo simulation of the tight-binding model of graphene with partially screened Coulomb interactions, *Phys. Rev. B* **89**, 195429 (2014).
- [18] M. Ulybyshev and S. Valgushev, Path integral representation for the Hubbard model with reduced number of Lefschetz thimbles, [arXiv:1712.02188](https://arxiv.org/abs/1712.02188).
- [19] W. Wu and A.-M. S. Tremblay, Phase diagram and Fermi liquid properties of the extended Hubbard model on the honeycomb lattice, *Phys. Rev. B* **89**, 205128 (2014).
- [20] P. Buividovich, D. Smith, M. Ulybyshev, and L. von Smekal, Numerical evidence of conformal phase transition in graphene with long-range interactions, *Phys. Rev. B* **99**, 205434 (2019).
- [21] T. O. Wehling, E. Şaşıoğlu, C. Friedrich, A. I. Lichtenstein, M. I. Katsnelson, and S. Blügel, Strength of Effective Coulomb Interactions in Graphene and Graphite, *Phys. Rev. Lett.* **106**, 236805 (2011).
- [22] W. Janke, Monte Carlo simulations in statistical physics from basic principles to advanced applications, *Order, Disorder and Criticality, Advanced Problems of Phase Transition Theory* (World Scientific, Singapore, 2012), pp. 93–166.
- [23] V. Sadovnichy, A. Tikhonravov, V. Voevodin, and V. Opanasenko, *Lomonosov: Supercomputing at Moscow State University* (Chapman & Hall/CRC Computational Science, Boca Raton, 2013), pp. 283–307.